Integration of DFIG-Based Wind Farms Into Series-Compensated Transmission Systems

Andres E. Leon, *Member, IEEE*

***Abstract*—Recent events have shown that doubly-fed induction generator (DFIG) wind turbines close to series capacitors are prone to subsynchronous oscillations (SSO). This paper analyzes these subsynchronous interactions (SSI) and a countermeasure to enable a reliable and secure integration of DFIG-based wind farms into series-compensated transmission systems. A case study based on a real power system is considered in this work. It has several transmission lines (many of them series compensated), various conventional and wind power plants, and a distributed load. This system allows to study the SSI among various wind farms and multiple subsynchronous modes, unlike previous studies which considered a single DFIG and one series-compensated line (i.e., one subsynchronous mode). An analytical investigation and development of fundamental concepts of the SSO are also discussed. A supplementary damping control (SDC) is designed to enhance the operating range and to damp the SSO of these series-compensated wind farms. A detailed analysis is carried out using eigenvalues and nonlinear time-domain simulations to evaluate the performance and robustness of the SDC. Besides the parameters usually studied, such as wind speed, series compensation level, control gains, the effects of conventional synchronous generation, type of load model, and system demand level on the SSI are also analyzed.**

***Index Terms*—Argentinian power system, series capacitor, sub-synchronous resonance, wind energy conversion systems.**

I. Introduction

WIND FARMS located far from load centers frequently require the update of the transmission infrastructure to accommodate the additional power [1]. From an economic point of view, in order to enhance the power transmission capacity and stability margin, series capacitor compensation of existing lines is usually preferred instead of building new lines [2]. However, fixed series capacitors present the risk of sub-synchronous interactions (SSI) [3] not only for the new power plants, but also for existing generation and power electronic equipment [4]. The SSI phenomenon was first discussed in 1937 [5] and received more attention in the 1970s, when two shaft failures occurred in the Mohave plant [6]. The potential interaction between wind farms and series capacitors was recognized a decade ago in [7]. Due to the increasing levels of wind generation, SSI events have been reported since 2009 in series-compensated doubly-fed induction generator (DFIG)-based wind farms in the south of Texas [8]–[11], southwest of Minnesota [12], [13], and north of China (Hebei province) [14]. These events showed that the power-electronic control system of the DFIG can present a negative resistance to the grid at sub-synchronous frequencies [15]. This phenomenon is called sub-synchronous control interaction (SSCI) [16]–[18] and results in a lower damping or instability of sub-synchronous oscillations (SSO), limiting therefore the penetration level of DFIG wind farms in series-compensated corridors.

To reduce the SSO, several authors proposed to use flexible ac transmission systems (FACTS), such as static var compensator, thyristor-controlled series capacitor, gate-controlled series capacitor or static synchronous compensator [19]–[25]. The main drawback of this approach is the cost of the FACTS device and its protection equipment. Other researches preferred to include a supplementary damping control (SDC) in the current control loop of the grid-side converter (GSC) [26]–[32]. This scheme presents some practical constraints that limit its effectiveness; for example, the GSC has a partial power rating (between 25% and 30% of the generator rating), and its power capability is mainly for the flow of the active power [33], [34]. In addition, the GSC currents have a controllability index of the sub-synchronous modes lower than the rotor-side converter (RSC) voltages (i.e., higher supplementary control action is necessary when using the GSC currents as control inputs [35]). Reference [36] proposed to mitigate the SSO reducing the gain of the rotor current controller, introducing measurement filters, and including an SDC in the RSC control loop. This method has the disadvantage that both the gain reduction and the low-pass filter action diminish the response time of the DFIG under disturbances. In [34], the authors modified the DFIG control structure by adding a derivative term and a low-pass filter with phase compensation to the RSC control. Then, to achieve a satisfactory performance for all the operating range, an additional SDC was also added to the GSC control. All these blocks and supplementary loops make this approach complicated, with several design stages. In [35], an SDC was designed using an optimal state-feedback technique based on a reduced model of the system. The main drawback of this procedure is that, when applied to an electrical network with multiple sub-synchronous modes, its performance can be sensitive to an accurate calculation of the reduced model. This can be solved by augmenting the order of the reduced model, at the expense of increasing the complexity of the control design.

Taking into account the above considerations, in practical power systems it could be more appropriate to gain in simplicity

Manuscript received June 20, 2015; revised October 12, 2015; accepted November 03, 2015. Date of publication December 01, 2015; date of current version March 18, 2016. This work was supported by Consejo Nacional de Investigaciones Científicas y Técnicas (CONICET) and Universidad Nacional del Sur. Paper no. TSTE-00528-2015.

The author is with the Instituto de Investigaciones en Ingeniería Eléctrica (IIIE) "Alfredo Desages" (UNS-CONICET), Universidad Nacional del Sur (DIEC-UNS), Bahía Blanca 8000, Argentina (e-mail: aleon@iiie-conicet.gob.ar).

Color versions of one or more of the figures in this paper are available online at http://ieeexplore.ieee.org.

Digital Object Identifier 10.1109/TSTE.2015.2498312

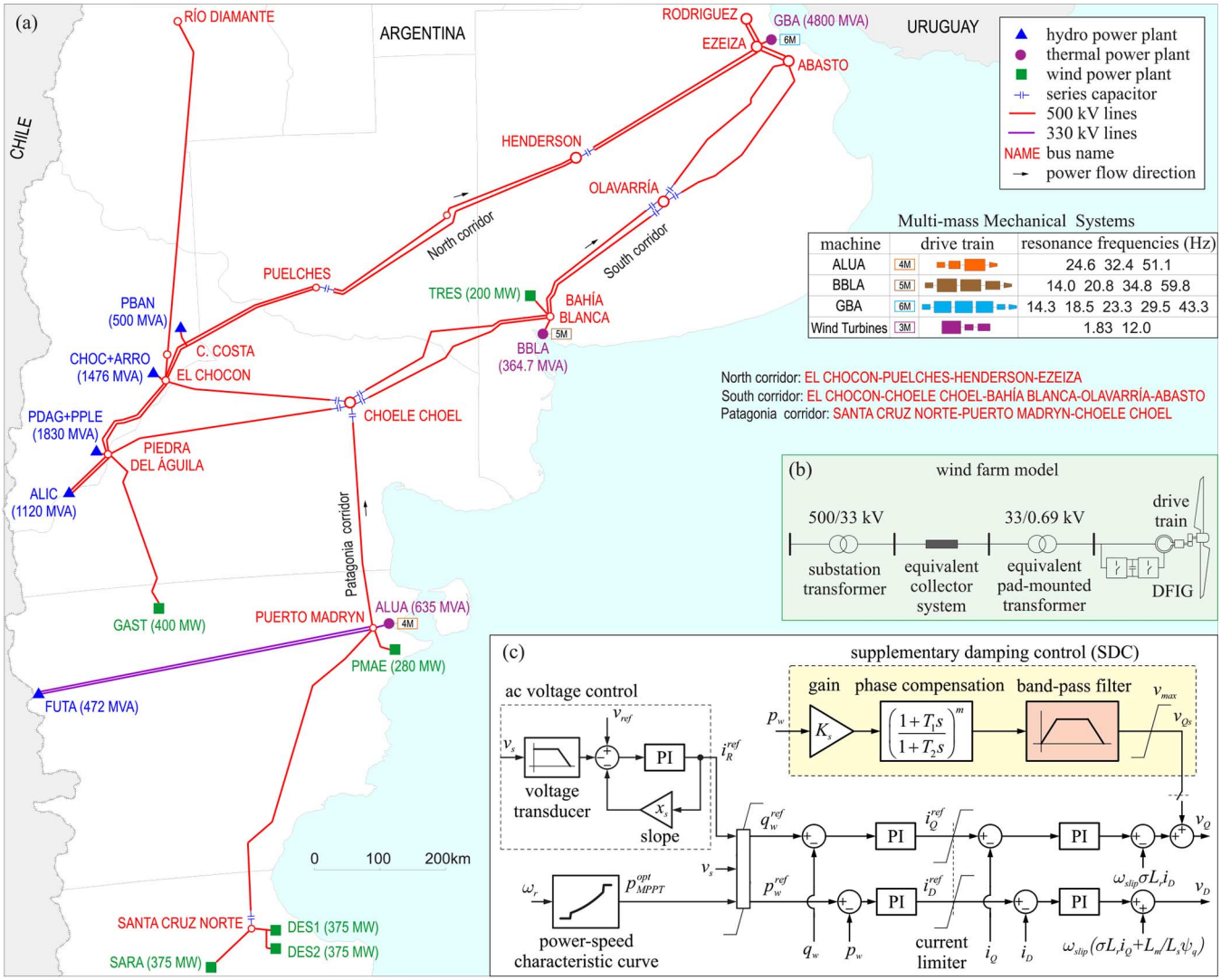

Fig. 1. Case study based on the Argentinian power system. (a) geographical and single-line diagram, (b) wind farm equivalent model, and (c) block diagram of the DFIG vector control and the implementation of the supplementary damping control (SDC).

and robustness using conventional control structures based on lead-lag compensators. The modification of the DFIG control algorithm by including an SDC (i.e., updating the control software) is a cost-effective solution, has a relatively quick implementation, and avoids the installation of expensive equipment such as FACTS or bypass filters [9]. In addition, if the SDC acts on the rotor voltage, it also has the advantage of directly aiming at the root of the SSCI problem, obtaining an excellent damping performance and high controllability of the sub-synchronous modes.

The power system used in previous works to study the SSI in wind farms usually presents some simplifications: (1) the electrical network consists of a single series-compensated line connected to an infinite bus, (2) the network has only one sub-synchronous mode, (3) a single DFIG is considered (or a few clusters are connected to a common bus, as part of the same wind farm), and (4) neither conventional power plants nor load buses are modeled. This work is focused on studying the SSI in electrical networks presenting both multiple series-compensated lines (i.e., various sub-synchronous modes) and multiple conventional and wind power plants, and on designing a countermeasure to mitigate the SSCI. Analytical expressions and development of fundamental concepts of the SSO are also discussed.

The main contributions of the paper are: (1) a case study based on a real power system is proposed to analyze the SSI in networks with multiple series capacitors, wind farms located in different places, conventional power plants, and the dynamics of a distributed load; (2) to reduce the SSCI, an SDC design methodology for DFIG wind turbines is validated in these systems with various sub-synchronous modes and several generating plants; (3) unlike previous works which studied system parameters such as wind speed, series compensation level, and control gains, the present work also analyzed the effect of conventional synchronous generation, type of load model, and system demand level on the SSO damping.

The paper is organized as follows. Section II introduces the considered case study. A description of the resonance frequencies in different network topologies is presented in Section III. Section IV describes the SSI using eigenvalues and modal tools.

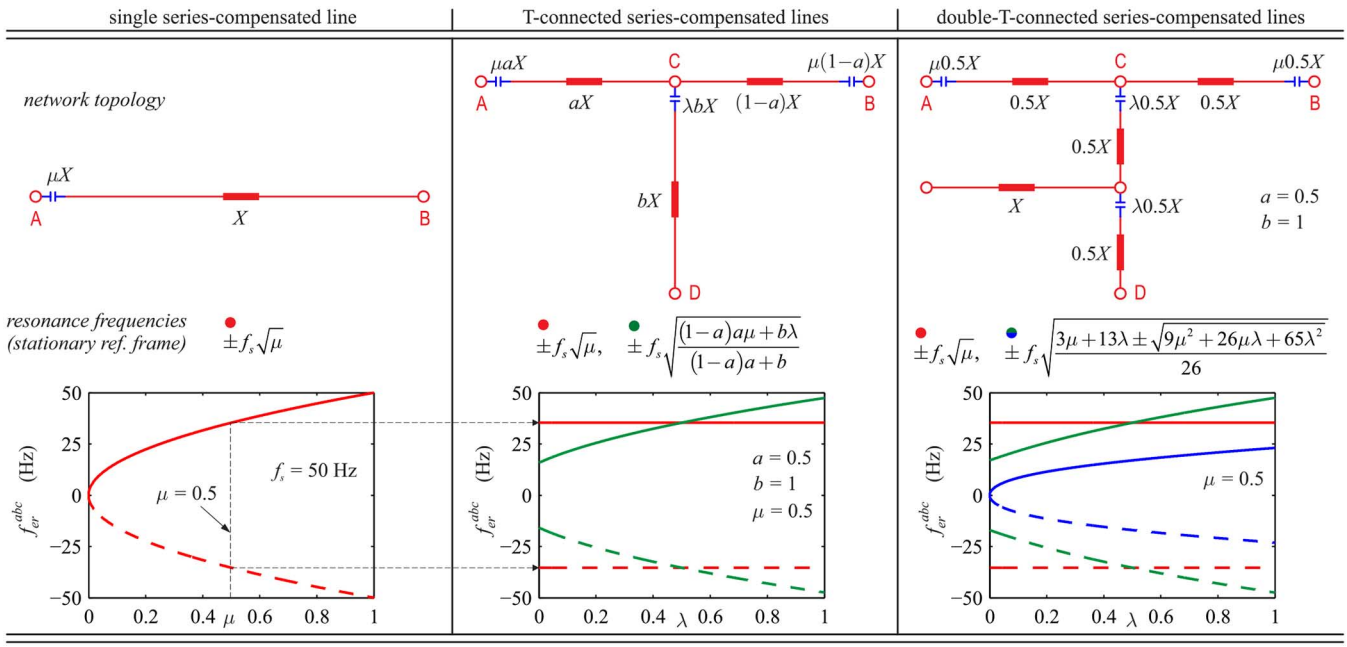

Fig. 2. Different electrical network topologies of series-compensated transmission systems, the analytical expressions of their resonance frequencies, and graphical representations of these frequencies as a function of the series compensation level.

In Section V, the control strategy to reduce the SSCI is developed. Small- and large-signal stability analyses are discussed in Sections VI and VII, respectively. Finally, conclusions are drawn in Section VIII.

II. Case Study

The case study was adapted from the Argentinian power system; it consists of 28 buses, 36 transmission lines, 12 series capacitors, 11 load buses, 8 conventional power plants, and 6 DFIG wind farms [see Fig. 1(a)]. Nowadays, the North and South corridors present a series compensation of 50%, and the Patagonia corridor is not compensated. However, a high compensation level for the last one is currently being analyzed by the Argentinian transmission system operator (TSO). This series capacitor compensation along with the large number of DFIG wind farms projected in the Patagonia corridor increase the risk of SSCI. The case study considered that both the series compensation of this corridor and the wind farms in planning stage had already been finished. This system allows to study a network with several elements and multiple sub-synchronous modes in a better way than the IEEE sub-synchronous resonance (SSR) benchmark models and other test systems usually considered in studies of series-compensated wind farms.

Synchronous generators were represented by detailed models [37] and were equipped with AVR, PSS, and governor systems. Thermal power plants also included a torsional filter [38]. The wind farm aggregated model consisted of the DFIG, turbine aerodynamic model, back-to-back voltage-source converters (average model), collector system, and pad-mounted and substation transformers [see Fig. 1(b)]. The RSC outer control loop included the maximum power point tracking and ac voltage control; the inner loop used a vector control to adjust the machine currents, whereas the GSC regulated the dc-link voltage. A schematic block diagram of the considered controllers is shown in Fig. 1(c) (see [39] for further details of wind turbine modeling and control).

To clarify the explanations and the presented results, and considering that hydro units have mechanical parameters that are less prone to SSR problems [3], the shaft of hydro generators was represented by a one-mass model. On the other hand, the shaft of both thermal and wind generators was represented by a multi-mass model. All mechanical systems and their resonance frequencies are shown in Table 'Multi-mass Mechanical Systems' inside Fig. 1. The transmission lines were modeled by π-circuits. The parameters of the generators and electrical network were taken from the reference guide of the Argentinian TSO, and shown in the Appendix.

The system dynamics was obtained by combining the ordinary differential equations of all the elements (e.g., synchronous generators, transmission lines, DFIGs, controls, etc.) involving 484 dynamic states. Then, after numerically calculating the equilibrium point and the Jacobian matrices, a modal analysis was computed following the expressions given in [38]. The small-signal analysis and the nonlinear time-domain simulations were performed using the MATLAB® 2014a software.

III. Resonances in Different Network Topologies

Figure 2 shows different topologies of series-compensated transmission systems. The first column presents a single series-compensated line, where f_s is the fundamental frequency of the system, X stands for the inductive reactance of the line, and μX is the capacitive reactance. The compensation level $\mu \in [0, 1]$ was defined as the ratio between the reactance of the series capacitor and the transmission line. In this case, the electrical resonance frequencies in the stationary reference frame are $f_{er}^{abc} = \pm f_s\sqrt{\mu}$; that is, the network resonates for

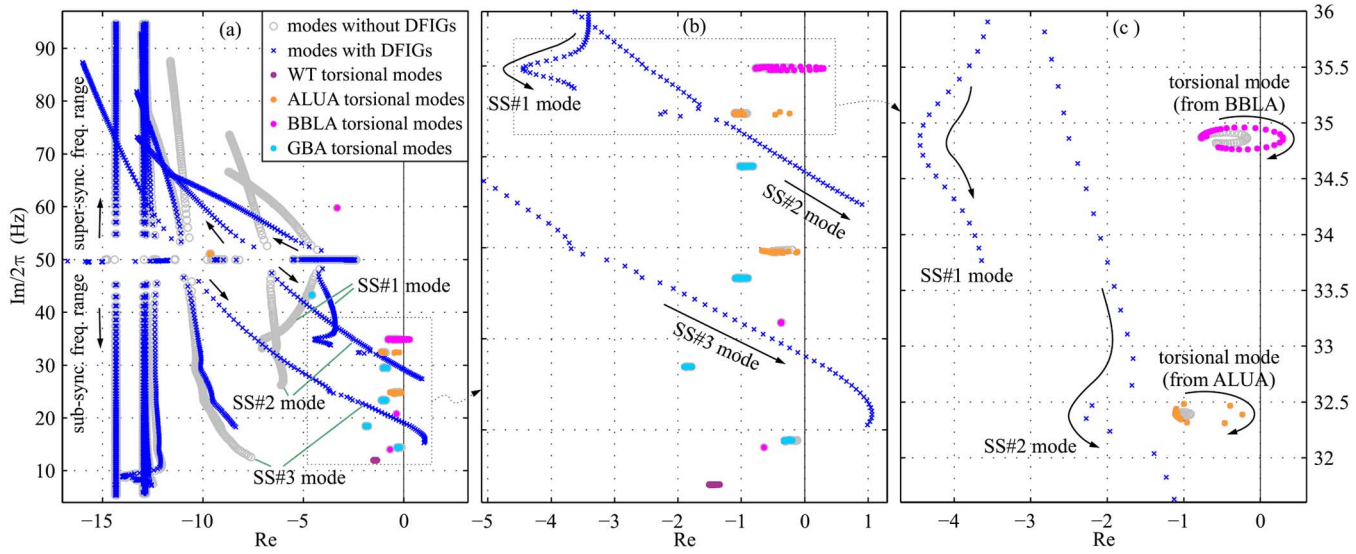

Fig. 3. Movement of the system eigenvalues when all the series compensations were varied from 1% to 80%. Electrical network modes (blue cross markers), shaft torsional modes (dot markers with different colors), and eigenvalues of the system without DFIG wind farms; that is, a system fully integrated by conventional generation (gray circle markers). (a) main view, and (b) and (c) zoom views.

both positive- and negative-sequence components at $f_s\sqrt{\mu}$ Hz (see solid and dashed lines in plots of Fig. 2). These frequencies in a synchronously rotating reference frame f_{er}^{dq} become $f_s - f_s\sqrt{\mu}$ and $f_s + f_s\sqrt{\mu}$, named sub- and super-synchronous frequencies, respectively.

The second column presents a series-compensated network in a T-connection. A second line C-D, whose connection point can be chosen with the parameter $a \in [0, 1]$, was added to the first transmission line A-B. The inductive reactance of the new line C-D is bX, and its compensation level is set by the parameter $\lambda \in [0, 1]$. In the T-connected series-compensated network, the original resonance frequencies $\pm f_s\sqrt{\mu}$ of the line A-B are still present, whereas a new pair of resonance frequencies arises due to the inclusion of the line C-D. These new frequencies are a function of various network parameters (see expression in the second column of Fig. 2). In order to show this result in a two-dimensional plot, it was assumed the following: the line C-D is connected to the middle point of the line A-B (i.e., $a = 0.5$), both lines have the same inductance ($b = 1$), and the line A-B is compensated at 50% ($\mu = 0.5$). At the bottom of the second column, the resonance frequencies are shown as a function of the parameter λ. Because the compensation level of the line A-B (μ) is fixed, the original resonance frequencies are constant (see red lines); on the other hand, the new pair of resonance frequencies varies with the series compensation level of the line C-D (see green lines). In this scenario, the electrical network presents four resonance frequencies: two sub-synchronous and two super-synchronous.

The third column of Fig. 2 introduces a more complex network in a double-T topology. In this case, a new line was connected to the middle point of the line C-D. For this network, besides the aforementioned frequencies, a third pair of resonance frequencies appears (see blue lines). Electrical networks with multiple series capacitors can present several sub-synchronous resonance frequencies which might interact with DFIG control systems and shaft torsional modes. These types of networks require a thorough analysis and broad solutions to mitigate the SSI phenomena.

IV. Description of the SSI

A. Eigenvalue Analysis

In this section, an eigenvalue analysis was used to characterize the SSI of the case study. Figure 3(a) shows the movement of the eigenvalues when all the series compensations of the system were varied from 1% to 80% [movement direction is indicated with arrows, and zoom views are shown in Figs. 3(b) and (c)]. Although this variation is not carried out in practice, this test was performed to better explain the SSI phenomena

Blue cross markers indicate the eigenvalues associated with the electrical network, dot markers of different colors indicate those associated with the mechanical systems (shaft torsional modes) [see labels in Fig. 3(a)], and gray circle markers indicate the eigenvalues of the system, in which all wind farms were replaced by synchronous generators (i.e., a power system fully integrated by conventional generation). In this way, cases with and without DFIGs were compared at the same power-flow operating point, and the impact of the DFIGs on the small-signal stability was observed.

In Fig. 3(a), when the series compensation levels are close to zero, as expected for non-compensated lines, the electrical network modes are around 50 Hz in the synchronous reference frame (i.e., the complement of 0 Hz in the stationary reference frame). When the series compensations grow, some network modes begin to fall, reducing their frequency (sub-synchronous modes), whereas others begin to rise, increasing their frequency (super-synchronous modes). When the first ones fall, they can reduce their damping ratio (causing poorly damped oscillations), cross the imaginary axis (losing their stability), or interact with shaft torsional modes (resulting in the classical torsional interaction (TI)-type SSR [3]).

TABLE I
MODAL ANALYSIS

Mode	f_{er}^{dq} (Hz)	ζ (%)	Local measurements with the highest observability index	RSC control inputs with the highest controllability index
SS#1	37.40	1.4	$p_w^{\mathtt{TRES}}(0.42)$, $\lvert i_{DQ}^{\mathtt{TRES}}\rvert(0.38)$, $\lvert i_{dq}^{\mathtt{TRES}}\rvert(0.30)$, $q_w^{\mathtt{TRES}}(0.30)$	$v_Q^{\mathtt{TRES}}(4.4)$, $v_D^{\mathtt{TRES}}(4.3)$, $v_D^{\mathtt{PMAE}}(0.7)$, $v_Q^{\mathtt{PMAE}}(0.7)$
SS#2	30.52	0.4	$p_w^{\mathtt{PMAE}}(0.29)$, $i_d^{\mathtt{PMAE}}(0.28)$, $i_D^{\mathtt{PMAE}}(0.27)$, $\lvert i_{DQ}^{\mathtt{PMAE}}\rvert(0.27)$	$v_Q^{\mathtt{PMAE}}(7.8)$, $v_D^{\mathtt{PMAE}}(7.5)$, $v_D^{\mathtt{DES1}}(5.6)$, $v_D^{\mathtt{DES2}}(5.6)$
SS#3	19.75	0.5	$p_w^{\mathtt{DES1}}(0.17)$, $p_w^{\mathtt{DES2}}(0.17)$, $i_d^{\mathtt{DES1}}(0.16)$, $i_d^{\mathtt{DES2}}(0.16)$	$v_D^{\mathtt{DES1}}(21)$, $v_D^{\mathtt{DES2}}(21)$, $v_D^{\mathtt{SARA}}(19.9)$, $v_Q^{\mathtt{DES1}}(17)$

In the case with DFIGs, some sub-synchronous modes (labeled SS#1, SS#2, and SS#3) move faster toward the right-half plane than in the case without DFIGs (worse oscillatory behavior), or even become unstable [compare blue cross markers with gray circle markers in Fig. 3(a)]. This damping reduction or instability of the sub-synchronous modes produced by the inclusion of DFIG wind farms is caused by the SSCI. As it will be shown in the next subsection, these sub-synchronous modes correspond to the series-compensated corridors which export a high percentage of wind power, or are near DFIG wind farms.

When the sub-synchronous mode SS#1 falls, it pushes the 34.8-Hz torsional mode of the BBLA generator toward the right-half plane [see Fig. 3(c)] causing, as a result, a TI-type SSR. A similar interaction is also observed in the same figure, between the sub-synchronous mode SS#2 and the 32.4-Hz torsional mode of the ALUA generator. Therefore, the inclusion of DFIG wind farms can also worsen the TI-type SSR in thermal power plants [compare colored dot markers with gray circle markers in Fig. 3(c)].

B. Modal Analysis

The wind farms which interacted with the sub-synchronous modes were identified using the participation factors [2]. The mode SS#1 was mainly affected by the dynamic states of the wind farm TRES, the mode SS#2 by those of the wind farm PMAE, and the mode SS#3 by those of the wind farms SARA, DES1, and DES2 [see wind farms in Fig. 1(a)]. This agreed with the modal analysis shown in Table I (calculated at the nominal operating point of the system), where the resonance frequency f_{er}^{dq}, damping ratio, and signals with the higher observability and controllability index of the main sub-synchronous modes are presented. Indeed, the best measurements and control inputs were those from the wind farms which mainly affected the corresponding sub-synchronous mode.

Participation factors also showed that the mode SS#1 was associated with variables of the South corridor, and modes SS#2 and SS#3 with variables of the Patagonia corridor. Note the analogy of the two sub-synchronous modes SS#2 and SS#3 with those of the network topology shown in the second column of Fig. 2, where $\lambda = 0$ and buses A, B, C, and D are CHOELE CHOEL, SANTA CRUZ NORTE, PUERTO MADRYN, and FUTA, respectively.

C. Physical Interpretation of the SSCI

In a DFIG, the sub-synchronous frequencies f_{er}^{abc} are usually lower than the electrical frequency corresponding to the rotor speed f_o; consequently, the slip at the sub-synchronous frequency $s_{ssr} = (f_{er}^{abc} - f_o)/f_{er}^{abc}$ is negative. As a result, viewed from the stator terminals, the equivalent rotor resistance $R_{eq}^{ssr} = R_r'/s_{ssr}$ is negative as well [40]. If R_{eq}^{ssr} exceeds the sum of the stator and network resistances, the system will have a negative damping at the sub-synchronous frequency, and growing oscillations will arise. This phenomenon is called induction generator effect (IGE), and only involves electrical dynamics [1]. In the rotor current control loop of the DFIG, the proportional gain of the PI controller can be interpreted as a resistance term added to the rotor circuit (see [14], [15], [34] and [41]). Therefore, this proportional gain increases the negative equivalent resistance R_{eq}^{ssr}, resulting in a lower damping or instability of the SSO. This aggravation of the IGE produced by the rotor current control loop is called SSCI, to differentiate it from the traditional IGE [16].

V. CONTROL STRATEGY TO REDUCE THE SSCI

To mitigate the adverse effects of DFIG wind farms on sub-synchronous modes, SDCs were added to the problematic wind farms. Their control structure is the classical gain with phase compensation widely used in power system applications [see yellow box in Fig. 1(c)]. A band-pass filter was also included to prevent steady-state operation and to avoid interactions with higher frequency modes. This SDC uses a local measurement (decentralized approach); therefore, neither communication links nor transmission time delays were involved. Besides, it was integrated into the RSC vector control, becoming more acceptable for system operators and manufacturers, who are usually conservative to fully replace the well-known control architectures.

This structure composed by lead-lag blocks is simpler, easier to tune, and more robust to uncertainties and changes in the system than more complex model-based approaches (such as linear-quadratic-gaussian controls, model predictive controls, etc.), which are more dependent on an accurate knowledge of the system.

A. Selection of the Measurement and Control Input

From the fourth column of Table I, the output active power of the wind farm (p_w) was chosen as measurement for the SDCs [29] (current could also be considered [21]). As control input, both d- and q-axis rotor voltages (v_D and v_Q) can be used to damp the SSO (see fifth column of Table I). The q-axis rotor voltage which acts on the reactive power control loop was chosen in order to minimize the impact of the SDC on the wind turbine mechanical system. For example, to damp the mode

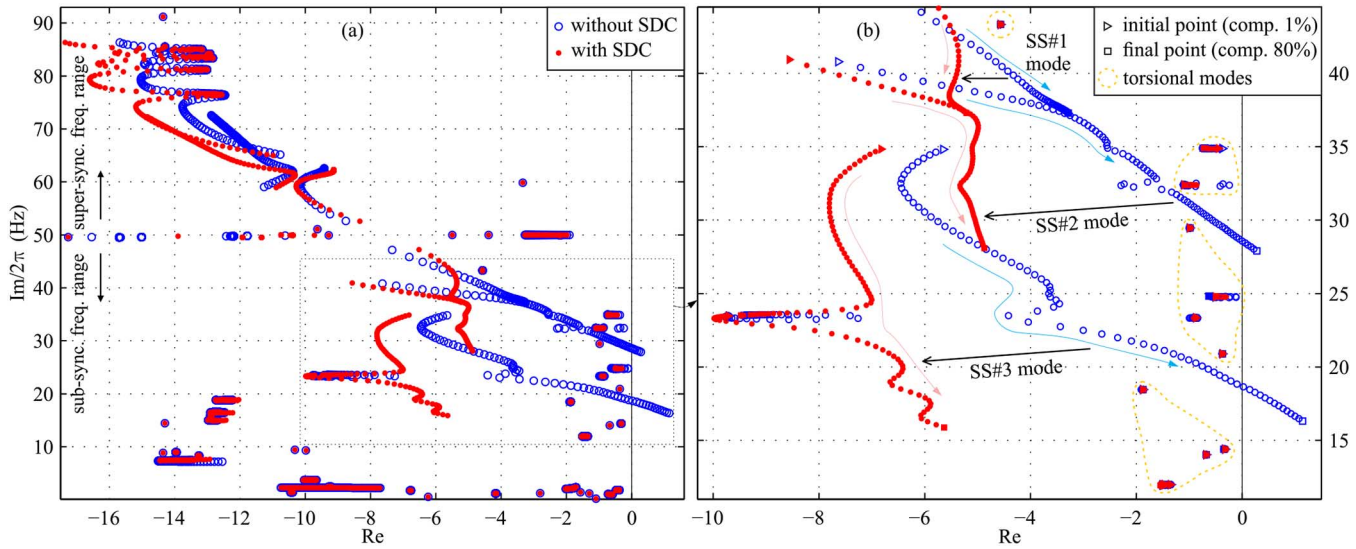

Fig. 4. Movement of the system eigenvalues when the series compensation of the Patagonia corridor was varied from 1% to 80%. System with the SDCs (red dot markers), and without the SDCs (blue circle markers). (a) main view, and (b) zoom view.

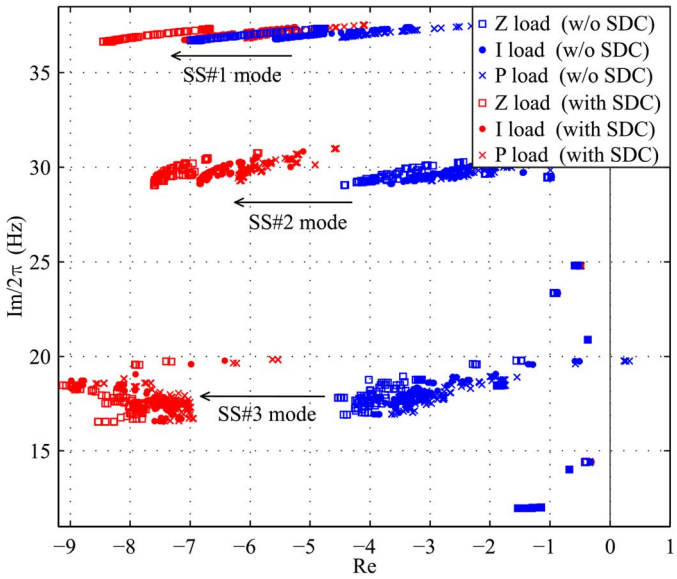

Fig. 5. Eigenvalues corresponding to all the considered wind conditions for three types of load behavior (i.e., constant Z, constant I and constant P load models indicated by square, dot, and cross markers, respectively). Cases with and without the SDCs are shown using red and blue markers, respectively.

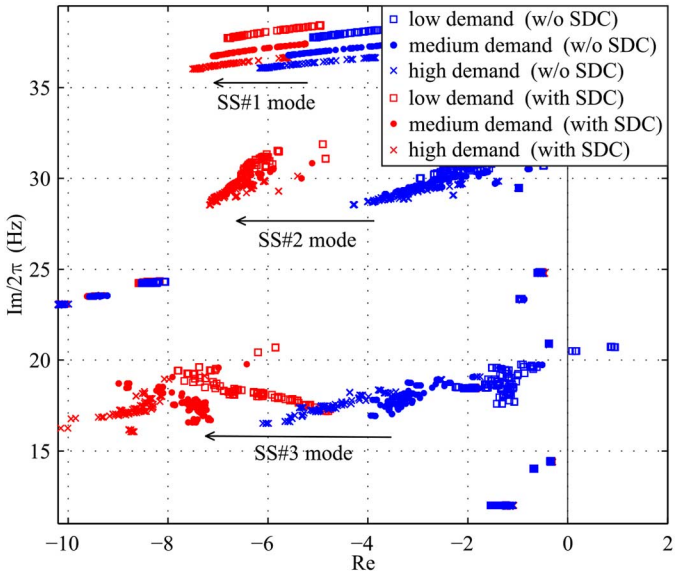

Fig. 6. Eigenvalues of all the considered wind conditions for three levels of system load (i.e., low, medium, and high demand indicated by square, dot, and cross markers, respectively). Cases with and without the SDCs are shown using red and blue markers, respectively.

SS#1, an SDC was added to the control system of the wind farm TRES. This control measures the active power p_w^{TRES}, and acts on the q-axis rotor voltage v_Q^{TRES}.

Although other signals with high controllability and observability could be used, these ones were chosen because they damp the sub-synchronous modes without destabilizing other system modes (e.g., electromechanical, torsional, and super-synchronous modes), and present a good closed-loop transient response.

B. Supplementary Damping Control (SDC) Design

The residue-based method was used to set the parameters of the SDC. First, the residue R_i corresponding to the target sub-synchronous eigenvalue $\sigma_i + j\omega_i$ was calculated. This eigenvalue was shifted toward the left-half plane in the 180° direction to increase its damping ratio. Therefore, the required phase compensation was $\phi = 180° - \arg(R_i)$. Then, the time constants of the lead-lag blocks were obtained from

$$\alpha = \frac{1 - \sin\frac{\phi}{m}}{1 + \sin\frac{\phi}{m}}, \qquad T_2 = \frac{1}{\omega_i\sqrt{\alpha}}, \qquad T_1 = \alpha T_2 \quad (1)$$

where m is the number of lead-lag blocks, usually $m = 2$ (see further details in [42]).

In the case study, SDCs were included in the wind farms TRES, PMAE, SARA, DES1, and DES2 to damp the critical sub-synchronous modes SS#1, SS#2 and SS#3. Each

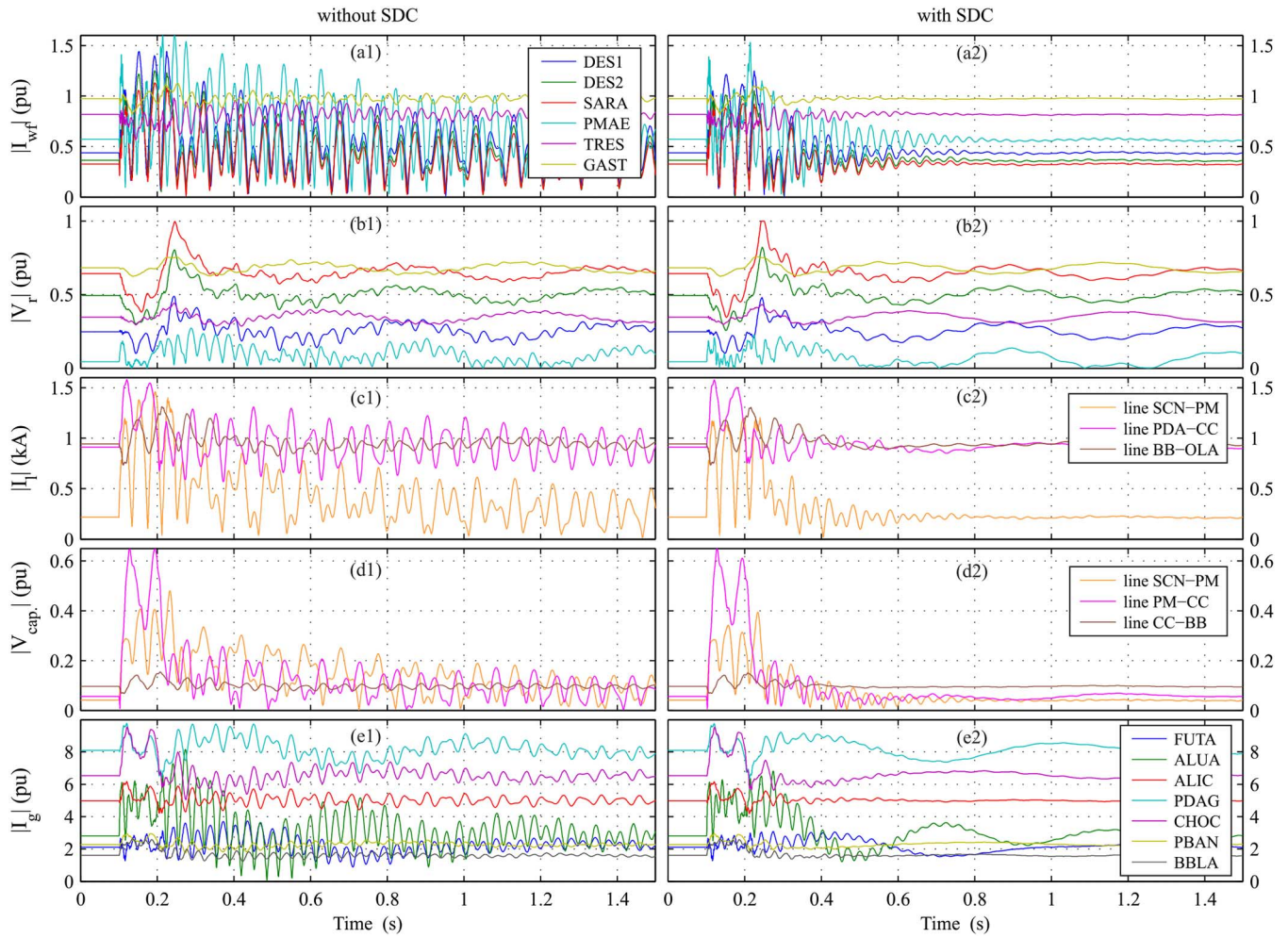

Fig. 7. Test considering a 100-ms three-phase fault at the bus PUERTO MADRYN. (a) output current of the wind farms, (b) DFIG rotor voltages, (c) current of the lines from SANTA CRUZ NORTE to PUERTO MADRYN, PIEDRA DEL ÁGUILA to CHOELE CHOEL, and one of the lines from BAHÍA BLANCA to OLAVARRÍA, (d) series capacitor voltage of the lines from SANTA CRUZ NORTE to PUERTO MADRYN, PUERTO MADRYN to CHOELE CHOEL, and one of the lines from CHOELE CHOEL to BAHÍA BLANCA, and (e) output current of conventional power plants (per-unit values on a 100 MVA base).

SDC was tuned in a poorly damped condition of the target sub-synchronous eigenvalue. From the SSCI point of view, this condition is obtained for low wind speeds and high series compensation levels [1]. In this way, good performance is provided under severe conditions whereas, for high wind speeds and low compensation levels, the SSCI is much less harmful (a similar criterion was also considered in [34]). As it will be shown in the next section, this control tuning presents high robustness for a wide range of operating conditions.

VI. Small-Signal Stability

In the following tests, the SDCs were tuned at a wind speed of 5.5 m/s, series compensation of 60% in the Patagonia corridor and medium demand level of the load (modeled as a constant-current source). The control parameters were kept constant for all the studied operating points (see Table V).

Figure 4(a) shows the movement of the eigenvalues when the series compensation of the Patagonia corridor was varied from 1% to 80%. The series compensation of both the North and South corridors was fixed in 50%. This test is useful to evaluate the robustness of the SDC when the compensation level seen from the wind farm bus varies under a contingency condition (like in the Texas event [11]). In the case without the SDCs, and analogously to what is shown in Fig. 3(a), the higher the series compensation level, the lower the damping ratios of the sub-synchronous modes. In fact, for high compensation levels some sub-synchronous modes became unstable. However, the inclusion of the SDCs was able to increase the damping ratios of the critical modes SS#1, SS#2 and SS#3 [see how they were moved toward the left in Fig. 4(b)]. Although the SDCs were tuned for a series compensation of 60% in the Patagonia corridor, they worked well for all the compensation range. At the same time, the damping ratios of the torsional modes in both wind and thermal power plants were not deteriorated by the action of the SDCs. Moreover, the 24.6-Hz and 32.4-Hz torsional modes were less affected by the interaction with the sub-synchronous network modes (i.e., lower TI-type SSR). On the other hand, TI phenomena were not evidenced in wind turbines, as explained in previous studies (see [2], [34] and [43]), because their poorly damped mechanical modes are generally at low frequencies, and very high series compensation levels are required to reach these low resonance modes.

The robustness against different types of load behavior was assessed by calculating the system eigenvalues for three load models [i.e., constant impedance (Z), constant current (I) and constant power (P)]. These models go from a soft dynamics (constant-Z load) to a hard dynamics (constant-P load). The wind speeds of the six wind farms were independently varied between low and high wind conditions, creating 100 different operating points randomly chosen. The results are shown in Fig. 5. In the cases without the SDCs (blue markers), some operating points were unstable (eigenvalues with positive real part). On the other hand, all cases with the SDCs (red markers) were stable, and the target eigenvalues had a more negative real part (see arrows in the critical sub-synchronous modes); therefore, the SSO damping was improved for all wind conditions, irrespectively of the load model.

Analogously to the previous test, Fig. 6 presents the system eigenvalues but, instead of studying different types of load behavior, different load power levels were considered (i.e., a low, medium, and high demand level of the system load). In this case, the inclusion of the SDCs also increased the damping ratios of the critical sub-synchronous modes in all wind conditions for different load power levels.

When considering the SSO damping, the worst-case scenarios were for the cases with a constant-P load model and a low demand level (see Figs. 5 and 6). When the load demand increased, more machines were dispatched in the conventional power plants, whereas it was assumed that the power delivered by the wind farms was kept constant, extracting the maximum power available from the wind. Figure 6 shows that when the demand level increased, the critical sub-synchronous modes had a more negative real part (better SSO damping). That is, the higher the power ratio between the conventional synchronous generation and the wind generation, the higher the damping ratio of the modes affected by the SSCI; consequently, the SSCI phenomenon is less harmful.

VII. Large-Signal Stability

Several nonlinear time-domain simulations were carried out to evaluate the transient response of the system under diverse operating conditions and different fault locations. Due to space limitations, only the most representative results are included.

In a first test, a 100-ms three-phase fault was applied at the bus PUERTO MADRYN. The system conditions were: a low demand level, series compensation of 60% in the Patagonia corridor, and constant-I load model. Figure 7 shows two cases: the system without and with the SDCs (first and second column, respectively). In the first case, after the disturbance, the output currents of the wind farms presented poorly damped sub-synchronous oscillations [see Fig. 7(a1)]. On the other hand, when the SDCs were activated, these oscillations were quickly damped [see Fig. 7(a2)]. It can also be seen that the voltage signal added by the SDC [control action v_{Qs} in Fig. 1(c)] slightly modified the rotor voltage magnitude, which remained within its allowed maximum limits [see Fig. 7(b2)]. The remaining 1.8 and 12 Hz oscillations in the rotor voltages are the wind turbine torsional modes (already present without the SDCs) which have longer settling times than the time window presented here. The

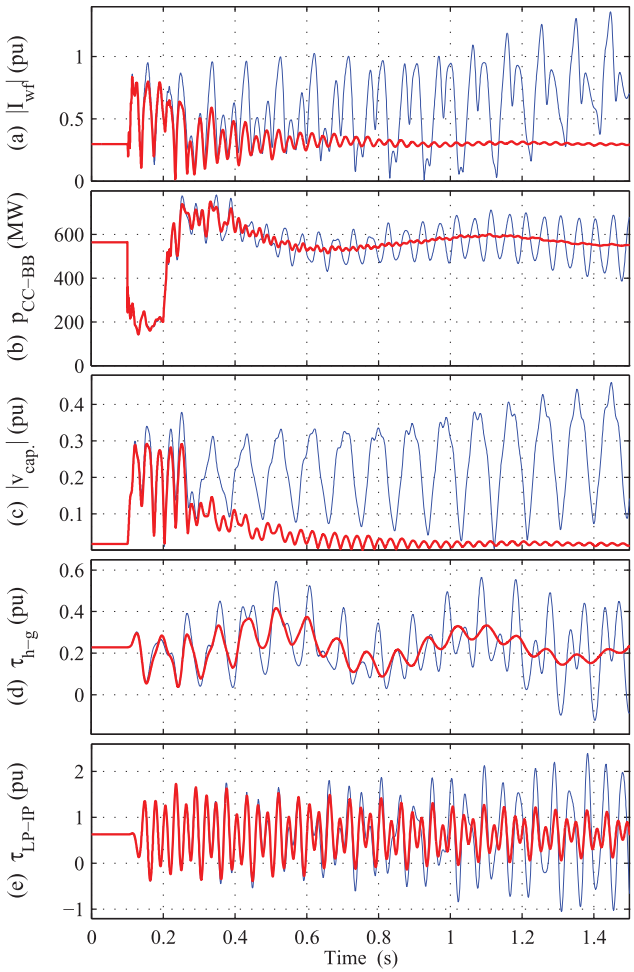

Fig. 8. Comparison of the power system response under a severe SSI condition, with and without the SDCs (red and blue lines, respectively). (a) output current of the wind farm DES1, (b) active power of one of the lines from CHOELE CHOEL to BAHÍA BLANCA, (c) series capacitor voltage of the SANTA CRUZ NORTE sub-station, (d) hub/generator shaft torque of the wind farm DES1, and (e) LP/IP shaft torque of the generator BBLA.

damping improvements of the sub-synchronous modes can also be observed in other system variables, such as line currents, series capacitor voltages, and generator currents [compare Figs. 7(c1)-(e1) with Figs. 7(c2)-(e2)].

In a second test, a more severe condition was analyzed by considering one of the unstable operating points obtained in Fig. 6 for low wind conditions. This time the fault was applied at the bus CHOELE CHOEL. Various electrical and mechanical variables are presented in Fig. 8. The improvements of the oscillation damping and stability are clear by comparing the cases with and without the SDCs (red and blue lines, respectively). Torsional stresses of both wind farms and synchronous generators were reduced when the SDCs were active, as seen from the amplitude (excursion) of their shaft torques in Fig. 8(d) and (e), respectively.

VIII. Conclusions

This paper analyzes the SSI in electrical networks with both multiple series-compensated lines (i.e., multiple

TABLE II
LINE DATA

Initial node	Final node	R	X	B	μ (%)
P. D. AGUILA	CH. CHOEL	0.00293	0.03612	4.669	40.4
EL CHOCON	CH. CHOEL	0.00244	0.02960	2.829	58.6
EL CHOCON	R. DIAMANTE	0.00253	0.03067	3.727	00.0
EL CHOCON	C. COSTA	0.00048	0.00520	1.941	00.0
C. COSTA	PUELCHES	0.00217	0.02358	2.231	00.0
C. COSTA	PUELCHES	0.00217	0.02358	2.231	00.0
PUELCHES	HENDERSON	0.00406	0.04524	4.445	50.7
PUELCHES	HENDERSON	0.00428	0.04640	4.388	50.7
HENDERSON	EZEIZA	0.00312	0.03415	3.279	68.1
HENDERSON	EZEIZA	0.00312	0.03415	3.279	68.1
CH. CHOEL	B. BLANCA	0.00308	0.03772	3.656	46.8
CH. CHOEL	B. BLANCA	0.00267	0.03272	4.195	42.3
B. BLANCA	OLAVARRIA	0.00232	0.02810	2.680	49.6
B. BLANCA	OLAVARRIA	0.00200	0.02419	3.051	40.3
OLAVARRIA	ABASTO	0.00263	0.03194	3.064	47.8
OLAVARRIA	ABASTO	0.00234	0.02852	3.624	46.0
ABASTO	EZEIZA	0.00055	0.00626	0.623	00.0
BBLA	B. BLANCA	0.00024	0.03641	0.289	00.0
TRES	B. BLANCA	0.00600	0.10655	1.074	00.0
ALIC	ALICURA	0.00000	0.01155	0.000	00.0
ALICURA	P. D. AGUILA	0.00035	0.00423	1.583	00.0
GAST	P. D. AGUILA	0.00558	0.08240	3.438	00.0
PDAG	P. D. AGUILA	0.00000	0.00820	0.000	00.0
P. D. AGUILA	EL CHOCON	0.00076	0.00910	3.436	00.0
CHOC	EL CHOCON	0.00000	0.01016	0.000	00.0
PBAN	C. COSTA	0.00027	0.03015	0.280	00.0
GBA	EZEIZA	0.00016	0.00313	0.000	00.0
FUTA	P. MADRYN 330kV	0.01167	0.10868	4.162	00.0
ALUA	P. MADRYN 330kV	0.00118	0.02360	0.000	00.0
P. MADRYN 330kV	P. MADRYN 500kV	0.00000	0.02962	0.000	00.0
PMAE	P. MADRYN 500kV	0.00369	0.06937	0.097	00.0
P. MADRYN 500kV	CH. CHOEL	0.00275	0.03384	4.189	60.0
P. MADRYN 500kV	S. C. NORTE	0.00401	0.05098	6.653	60.0
DES1	S. C. NORTE	0.00282	0.05253	0.145	00.0
DES2	S. C. NORTE	0.00282	0.05253	0.145	00.0
SARA	S. C. NORTE	0.00382	0.06380	1.268	00.0

► Parameters are in p.u. on a 100 MVA base.

sub-synchronous modes) and DFIG wind farms. With this aim, a case study was considered based on a real power system presenting several series capacitors, various conventional and wind power plants, distributed loads, and multiple torsional modes.

From previous works, it is known that the SSCI is aggravated for low wind speeds, high series compensation levels, and high gains of the rotor current controller. From the obtained results, it was found that the SSCI is also aggravated for loads with a hard dynamics (i.e., a constant-P type behavior), and for low demand levels of the system load. It was also noticed that the presence of conventional synchronous generation attenuates the SSCI. Therefore, it is expected that this interaction will be lower in networks with coexistence of different types of generation systems than in those scenarios with prevalence of (or only) DFIG-based generation.

To reduce the adverse effects of SSCI and ensure a reliable integration of DFIG wind farms into series-compensated transmission systems, a supplementary damping control was also investigated. Using a modal analysis, the optimal wind farms and signals to perform the supplementary actions were identified. The results show that the considered control scheme can significantly and robustly damp the sub-synchronous modes in practical power systems under different operating conditions.

TABLE III
GENERATOR DATA

Generator	FUTA	ALUA	ALIC	PDAG	CHOC	PBAN	BBLA	GBA
S_B (MVA)	472.0	635.6	1120	1830	1476	500.0	364.7	4800
V_B (kV)	13.80	11.00	13.80	15.40	16.00	16.00	20.00	13.80
type	hydro	thermal	hydro	hydro	hydro	hydro	thermal	thermal
x_l	0.130	0.170	0.130	0.160	0.130	0.130	0.150	0.106
r_s	0.003	0.003	0.003	0.003	0.003	0.003	0.003	0.003
x_d	1.050	2.705	0.800	0.966	1.100	1.060	1.700	2.050
x'_d	0.290	0.284	0.260	0.352	0.216	0.216	0.300	0.257
x''_d	0.200	0.183	0.170	0.245	0.155	0.155	0.250	0.158
t'_{d0} (s)	9.630	5.980	8.525	11.11	5.700	5.700	6.000	6.000
t''_{d0} (s)	0.054	0.032	0.050	0.158	0.064	0.064	0.050	0.035
x_q	0.610	2.437	0.600	0.631	0.730	0.731	1.450	2.050
x'_q	0.609	0.345	0.599	0.630	0.729	0.730	0.350	0.515
x''_q	0.200	0.183	0.170	0.245	0.155	0.155	0.250	0.158
t'_{q0} (s)	0.001	0.700	0.001	0.001	0.001	0.001	0.500	0.900
t''_{q0} (s)	0.102	0.034	0.070	0.194	0.080	0.080	0.050	0.070
$M = 2H$ (s)	8.640	8.000	9.000	10.05	9.440	10.56	5.940	7.100
$x_{\text{transformer}}$	0.116	0.150	0.130	0.150	0.150	0.136	0.121	0.150

► Except where indicated, parameters are in p.u. on the generator base.

TABLE IV
LOAD DATA

Load bus	P (MW)	Q (MVA)	Load bus	P (MW)	Q (MVA)
OLAVARRIA	400	100	ALICURA	122	31
B. BLANCA	371	93	S. C. NORTE	80	20
HENDERSON	320	80	CH. CHOEL	20	5
P. MADRYN 330kV	703	176	PUELCHES	30	8
EZEIZA/ABASTO	6700	300	R. DIAMANTE	750	188

TABLE V
SDC PARAMETERS

Wind farm	DES1	DES2	SARA	PMAE	TRES
SDC loop gain	0.0500	0.0500	0.0500	0.0750	0.0750
Lead time constant T_1 (s)	0.0207	0.0207	0.0221	0.0134	0.0155
Lag time constant T_2 (s)	0.0031	0.0031	0.0029	0.0020	0.0012
Pass-band frequency (Hz)	10	10	10	15	25
Stop-band frequency (Hz)	35	35	35	45	45

► SDCs have two lead-lag blocks (i.e., $m = 2$).

APPENDIX

The line, synchronous generator, and load data are shown in Tables II, III, and IV, respectively; whereas the SDC parameters are presented in Table V.

REFERENCES

[1] H. Mohammadpour and E. Santi, "Sub-synchronous resonance analysis in DFIG-based wind farms: Definitions and problem identification—Part I," in *Proc. IEEE Energy Convers. Congr. Expos.*, Sep. 2014, pp. 812–819.

[2] D. Suriyaarachchi, U. Annakkage, C. Karawita, and D. Jacobson, "A procedure to study subsynchronous interactions in wind integrated power systems," *IEEE Trans. Power Syst.*, vol. 28, no. 1, pp. 377–384, Feb. 2013.

[3] IEEE Committee Report, "Reader's guide to subsynchronous resonance," *IEEE Trans. Power Syst.*, vol. 7, no. 1, pp. 150–157, Feb. 1992.

[4] A. E. Leon, J. M. Mauricio, and J. A. Solsona, "Subsynchronous resonance mitigation using variable-speed wind energy conversion systems," *IET Gener. Transmiss. Distrib.*, vol. 7, no. 5, pp. 511–525, May 2013.

[5] J. W. Butler and C. Concordia, "Analysis of series capacitor application problems," *Trans. AIEE*, vol. 56, no. 8, pp. 975–988, Aug. 1937.

[6] D. Walker, C. Bowler, R. Jackson, and D. Hodges, "Results of subsynchronous resonance test at Mohave," *IEEE Trans. Power Appl. Syst.*, vol. 94, no. 5, pp. 1878–1889, Sep. 1975.

[7] P. Pourbeik, R. Koessler, D. Dickmander, and W. Wong, "Integration of large wind farms into utility grids (Part 2—Performance issues)," in *Proc. IEEE Power Eng. Soc. Gen. Meeting*, 2003, vol. 3, pp. 1520–1525.
[8] D. Kidd and P. Hassink, "Transmission operator perspective of subsynchronous interaction," in *Proc. IEEE PES Transmiss. Distrib. Conf. Expo.*, 2012, pp. 1–3.
[9] J. Daniel *et al.*, "ERCOT CREZ reactive power compensation study," ABB Inc., Power Systems Division, Grid Systems Consulting, Raleigh, NC, Rep. No. E3800-PR-02, 2010.
[10] M. Bongiorno, A. Petersson, and E. Agneholm, "The impact of wind farms on subsynchronous resonance in power systems," Elforsk AB, Stockholm, Rep. V-309, Apr. 2011.
[11] J. Adams, C. Carter, and S.-H. Huang, "ERCOT experience with subsynchronous control interaction and proposed remediation," in *Proc. IEEE PES Transmiss. Distrib. Conf. Expo.*, 2012, pp. 1–5.
[12] K. Narendra *et al.*, "New microprocessor based relay to monitor and protect power systems against sub-harmonics," in *Proc. IEEE Elect. Power Energy Conf. (EPEC'11)*, 2011, pp. 438–443.
[13] R. Varma and A. Moharana, "SSR in double-cage induction generator-based wind farm connected to series-compensated transmission line," *IEEE Trans. Power Syst.*, vol. 28, no. 3, pp. 2573–2583, Aug. 2013.
[14] L. Wang, X. Xie, Q. Jiang, H. Liu, Y. Li, and H. Liu, "Investigation of SSR in practical DFIG-based wind farms connected to a series-compensated power system," *IEEE Trans. Power Syst.*, vol. 30, no. 5, pp. 2772–2779, Sep. 2015.
[15] E. Larsen, "Wind generators and series-compensated AC transmission lines," in *Proc. IEEE PES Transmiss. Distrib. Conf. Expo.*, 2012, pp. 1–4.
[16] L. C. Gross, "Sub-synchronous grid conditions: New event, new problem, and new solutions," in *Proc. Western Protective Relay Conf.*, 2010, pp. 1–19.
[17] B. Badrzadeh, M. Sahni, Y. Zhou, D. Muthumuni, and A. Gole, "General methodology for analysis of sub-synchronous interaction in wind power plants," *IEEE Trans. Power Syst.*, vol. 28, no. 2, pp. 1858–1869, May 2013.
[18] T. Ackermann and R. Kuwahata, "Lessons learned from international wind integration studies," AEMO wind integration WP4(A). Commissioned by Australian Energy Market Operator, 2011.
[19] R. Varma, S. Auddy, and Y. Semsedini, "Mitigation of subsynchronous resonance in a series-compensated wind farm using FACTS controllers," *IEEE Trans. Power Del.*, vol. 23, no. 3, pp. 1645–1654, Jul. 2008.
[20] M. El-Moursi, B. Bak-Jensen, and M. Abdel-Rahman, "Novel STATCOM controller for mitigating SSR and damping power system oscillations in a series compensated wind park," *IEEE Trans. Power Electron.*, vol. 25, no. 2, pp. 429–441, Feb. 2010.
[21] D. Suriyaarachchi, U. Annakkage, C. Karawita, D. Kell, R. Mendis, and R. Chopra, "Application of an SVC to damp sub-synchronous interaction between wind farms and series compensated transmission lines," in *Proc. IEEE Power Energy Soc. Gen. Meeting*, Jul. 2012, pp. 1–6.
[22] A. Moharana, R. Varma, and R. Seethapathy, "SSR alleviation by STATCOM in induction-generator-based wind farm connected to series compensated line," *IEEE Trans. Sustain. Energy*, vol. 5, no. 3, pp. 947–957, Jul. 2014.
[23] H. Mohammadpour, A. Ghaderi, and E. Santi, "Analysis of subsynchronous resonance in doubly-fed induction generator-based wind farms interfaced with gate-controlled series capacitor," *IET Gener. Transmiss. Distrib.*, vol. 8, no. 12, pp. 1998–2011, 2014.
[24] L. Piyasinghe, Z. Miao, J. Khazaei, and L. Fan, "Impedance model-based SSR analysis for TCSC compensated type-3 wind energy delivery systems," *IEEE Trans. Sustain. Energy*, vol. 6, no. 1, pp. 179–187, Jan. 2015.
[25] H. Mohammadpour and E. Santi, "Modeling and control of gate-controlled series capacitor interfaced with a DFIG-based wind farm," *IEEE Trans. Ind. Electron.*, vol. 62, no. 2, pp. 1022–1033, Feb. 2015.
[26] C. Zhu, L. Fan, and M. Hu, "Control and analysis of DFIG-based wind turbines in a series compensated network for SSR damping," in *Proc. IEEE Power Energy Soc. Gen. Meeting*, 2010, pp. 1–6.
[27] L. Fan, C. Zhu, Z. Miao, and M. Hu, "Modal analysis of a DFIG-based wind farm interfaced with a series compensated network," *IEEE Trans. Energy Convers.*, vol. 26, no. 4, pp. 1010–1020, Dec. 2011.
[28] L. Fan and Z. Miao, "Mitigating SSR using DFIG-based wind generation," *IEEE Trans. Sustain. Energy*, vol. 3, no. 3, pp. 349–358, Jul. 2012.
[29] U. Karaagac, S. Faried, J. Mahseredjian, and A.-A. Edris, "Coordinated control of wind energy conversion systems for mitigating subsynchronous interaction in DFIG-based wind farms," *IEEE Trans. Smart Grid*, vol. 5, no. 5, pp. 2440–2449, Sep. 2014.
[30] H. Mohammadpour and E. Santi, "SSR damping controller design and optimal placement in rotor-side and grid-side converters of series-compensated DFIG-based wind farm," *IEEE Trans. Sustain. Energy*, vol. 6, no. 2, pp. 388–399, Apr. 2015.
[31] H. A. Mohammadpour, A. Ghaderi, H. Mohammadpour, and E. Santi, "SSR damping in wind farms using observed-state feedback control of DFIG converters," *Elect. Power Syst. Res.*, vol. 123, pp. 57–66, 2015.
[32] H. Mohammadpour and E. Santi, "Optimal adaptive sub-synchronous resonance damping controller for a series-compensated doubly-fed induction generator-based wind farm," *IET Renew. Power Gener.*, vol. 9, no. 6, pp. 669–681, 2015.
[33] H. Xie, B. Li, C. Heyman, M. de Oliveira, and M. Monge, "Subsynchronous resonance characteristics in presence of doubly-fed induction generator and series compensation and mitigation of subsynchronous resonance by proper control of series capacitor," *IET Renew. Power Gener.*, vol. 8, no. 4, pp. 411–421, May 2014.
[34] P.-H. Huang, M. El Moursi, W. Xiao, and J. Kirtley, "Subsynchronous resonance mitigation for series-compensated DFIG-based wind farm by using two-degree-of-freedom control strategy," *IEEE Trans. Power Syst.*, vol. 30, no. 3, pp. 1442–1454, May 2015.
[35] A. E. Leon and J. A. Solsona, "Sub-synchronous interaction damping control for DFIG wind turbines," *IEEE Trans. Power Syst.*, vol. 30, no. 1, pp. 419–428, Jan. 2015.
[36] G. Irwin, A. Jindal, and A. Isaacs, "Sub-synchronous control interactions between type 3 wind turbines and series compensated AC transmission systems," in *Proc. IEEE Power Energy Soc. Gen. Meeting*, Jul. 2011, pp. 1–6.
[37] P. C. Krause, *Analysis of Electric Machinery*. New York, NY, USA: McGraw-Hill, 1995.
[38] P. Kundur, *Power System Stability and Control*. New York, NY, USA: McGraw-Hill, 1994.
[39] O. Anaya-Lara, N. Jenkins, J. Ekanayake, P. Cartwright, and M. Hughes, *Wind Energy Generation: Modelling and Control*. Hoboken, NJ, USA: Wiley, 2009.
[40] C. Zhu, M. Hu, and Z. Wu, "Parameters impact on the performance of a double-fed induction generator-based wind turbine for subsynchronous resonance control," *IET Renew. Power Gener.*, vol. 6, no. 2, pp. 92–98, 2012.
[41] J. Daniel, W. Wong, G. Ingestrom, and J. Sjoberg, "Subsynchronous phenomena and wind turbine generators," in *Proc. IEEE PES Transmiss. Distrib. Conf. Expo.*, May 2012, pp. 1–6.
[42] M. Aboul-Ela, A. Sallam, J. McCalley, and A. Fouad, "Damping controller design for power system oscillations using global signals," *IEEE Trans. Power Syst.*, vol. 11, no. 2, pp. 767–773, May 1996.
[43] L. Fan, R. Kavasseri, Z. L. Miao, and C. Zhu, "Modeling of DFIG-based wind farms for SSR analysis," *IEEE Trans. Power Del.*, vol. 25, no. 4, pp. 2073–2082, Oct. 2010.

Andres E. Leon (S'05–M'13) received the B.S. degree in electrical engineering from the Universidad Nacional del Comahue, Neuquén, Argentina, and the Ph.D. degree in control systems from the Universidad Nacional del Sur, Bahía Blanca, Argentina, in 2005 and 2011, respectively. Since 2012, he has been with the National Scientific and Technical Research Council (CONICET), as a Researcher. He is currently working with the Research Institute of Electrical Engineering "Alfredo Desages" (IIIE), Bahía Blanca, Argentina. His research interests include power system control and wind energy conversion systems.